

Exploring the Beam Energy Dependence of Flow-Like Signatures in Small System d +Au Collisions

J.D. Orjuela Koop, R. Belmont, P. Yin, J.L. Nagle¹

¹*University of Colorado Boulder, Boulder, Colorado 80309, USA*

(Dated: May 4, 2016)

Recent analyses of small collision systems, namely $p+p$ and $p+\text{Pb}$ at the LHC, and $p+\text{Au}$, $d+\text{Au}$ and $^3\text{He}+\text{Au}$ at RHIC, have revealed azimuthal momentum anisotropies commonly associated with collective flow in larger systems. Viscous hydrodynamics and parton cascade calculations have proven successful at describing some flow-like observables in these systems. These two classes of calculations also confirm these observables to be directly related to the initial geometry of the created system. Describing data at the highest RHIC and LHC energies requires a quark-gluon plasma or partonic rescattering stage, which raises the question of how small and low in energy can one push the system before only hadronic interactions are required for a full description. Hence, a beam energy scan of small systems—that amounts to varying the initial temperature and the lifetime of the medium—can provide valuable information to shed light on these issues. In this paper, we present predictions from viscous hydrodynamics (SONIC and SUPERSONIC), and partonic (AMPT) and hadronic (URMQD) cascade calculations for elliptic (v_2) and triangular (v_3) anisotropy coefficients in $d+\text{Au}$ collisions at $\sqrt{s_{NN}} = 7.7, 20, 39, 62.4, 200$ GeV and 5.02 TeV.

PACS numbers: 25.75.Gz, 25.75.Gz.Ld

I. INTRODUCTION

A major achievement in the field of ultrarelativistic heavy ion collisions has been the discovery that nuclear matter in its deconfined state above the transition temperature—also known as the Quark-Gluon Plasma (QGP)—behaves as a locally equilibrated, strongly coupled fluid [1]. Evidence for this claim comes from the azimuthal momentum anisotropy of emitted particles with respect to the event plane of the collision Ψ_n , as quantified by flow coefficients v_n ,

$$v_n = \langle \cos[n(\phi - \Psi_n)] \rangle. \quad (1)$$

where $n = 2$ ($n = 3$) corresponds to elliptic (triangular) flow coefficients. Nearly inviscid hydrodynamics has proven to be a powerful theoretical framework to understand the physics of the medium following thermalization [2]. It can explain the dependence of v_n on particle transverse momentum p_T , particle species, collision centrality, and collision energy. However, despite great success in understanding the bulk dynamics of the QGP, the question of its formation remains open, and stronger experimental constraints on pre-equilibrium dynamics and alternative dynamical scenarios are needed.

To that end, the Relativistic Heavy Ion Collider (RHIC) and the Large Hadron Collider (LHC) pursued a small systems program (i.e., $d+\text{Au}$ and $p+\text{Pb}$ respectively), originally aimed at elucidating the impact of cold nuclear matter effects on QGP formation. However, it was discovered that these systems [3–7], including most recently $p+p$ collisions at $\sqrt{s_{NN}} = 13$ TeV [8, 9], also exhibit azimuthal anisotropies reminiscent of those in $\text{A}+\text{A}$ collisions. Namely, a near-side ($\Delta\phi \approx 0$) enhancement in two particle correlations is visible even when imposing a large pseudorapidity separation to minimize contribu-

tions to the signal from jet fragmentation and other non-flow sources.

This observation challenges the conventional understanding of how big a droplet of matter is required to form a QGP. It also raises the question of whether—and under what conditions—a hydrodynamic description is applicable in this new regime. Hence, further studies were carried out at RHIC using $p+\text{Au}$ and $^3\text{He}+\text{Au}$ to disentangle initial-state effects, pre-equilibrium dynamics, and final-state effects in the development of the observed flow-like signals, by leveraging the distinct intrinsic elliptic ($d+\text{Au}$) and triangular ($^3\text{He}+\text{Au}$) geometry of these systems [10, 11].

Studies showed that nearly inviscid hydrodynamics, as implemented in the SONIC model [12], provides a good description of the measured v_2 in $d+\text{Au}$, $^3\text{He}+\text{Au}$, and most recently in $p+\text{Au}$ [13], as well as v_3 in $^3\text{He}+\text{Au}$ [11]. Furthermore, including a pre-equilibrium flow stage, as present in the SUPERSONIC model [14], results in a closer agreement with experimental data, with the largest influence in triangular flow.

However, it was also shown that completely different physics, as encoded in A-Multi-Phase-Transport (AMPT) model with a modest parton-parton cross section, can reproduce the observed two-particle correlations [15] and anisotropy coefficients [16] in $p+\text{Pb}$ and $p+p$ at the LHC, as well as the measured v_2 and v_3 for $p_T < 1$ GeV/c in $p+\text{Au}$, $d+\text{Au}$, and $^3\text{He}+\text{Au}$ at RHIC [17]. In this context, the physics responsible for the development of azimuthal momentum anisotropy—although not yet fully understood—has been identified to be a combination of rather limited partonic scattering and freeze out [18], and a simple coordinate space coalescence followed by hadronic scattering [17].

The Ultra-Relativistic Quantum Molecular Dynamics (URQMD) model is another theoretical framework that

has been utilized to understand flow in small systems [19], although it typically does not describe v_n values for large collision systems at $\sqrt{s_{NN}} = 200$ GeV [20]. Since URQMD does not include any partonic or QGP stage, it is an excellent comparison model to the above calculations.

Although the above studies have provided substantial insight into the role of initial geometry in small system anisotropies, further study is required to fully understand how the azimuthal anisotropy accrues in these short-lived systems, since they do not live long enough to fully translate initial-state geometry to final-state momentum anisotropy. Pre-equilibrium dynamics as well as later stage hadronic interactions are expected to play a larger role than in A+A collisions [14, 19]. To that end, the RHIC program is planning to include a small system beam energy scan in its 2016 run period, colliding d +Au at a variety of center-of-mass energies from $\sqrt{s_{NN}} = 20$ to 200 GeV.

In this paper, we utilize the theoretical frameworks—(SUPER)SONIC and AMPT—that provide a reasonable agreement with currently available datasets, to make predictions for elliptic and triangular Fourier coefficients, v_2 and v_3 , for d +Au at $\sqrt{s_{NN}} = 7.7, 20, 39, 62.4$, and 200 GeV, as well as d +Pb at $\sqrt{s_{NN}} = 5.02$ TeV. We also present v_2 results from URQMD at these energies. We begin by describing the AMPT, URQMD, and (SUPER)SONIC models, as well as the methodology used to compute v_n . We then present and compare the results for all energies obtained with the three models. Finally, we discuss the results and draw conclusions from them.

II. MODEL CALCULATIONS

A. AMPT

The AMPT generator [21] has been established as a useful tool in the study of heavy ion collisions. In AMPT, initial conditions are generated using a Monte Carlo Glauber model as implemented in the HIJING generator [22]. Zhang’s Parton Cascade (ZPC) is then used to model partonic scattering, with a parton-parton interaction cross section inversely proportional to the parton screening mass. Hadronization is implemented as a simple coordinate space coalescence, where the closest particle pairs and triplets are bound into mesons and baryons, respectively. Lastly, the model incorporates a hadronic scattering phase using A-Relativistic-Transport (ART).

In this paper, we follow the methodology of Ref. [17] and use AMPT Version 2.26 with string melting turned on. It is notable that in the string melting case, all partons are quarks and anti-quarks in the exact number to provide the constituent quarks of the final state hadrons via coalescence. A momentum dependent formation time for these (anti)quarks is implemented, effectively giving them a brief free streaming time that generates an initial space-momentum correlation. This mechanism plays an important role within AMPT on the final momentum

anisotropies.

We have modified the default AMPT Monte Carlo Glauber to sample the positions of the deuteron nucleons from the Hulthén wavefunction description of the nucleus. Additionally, we modified the initial nucleon interactions from the default HIJING implementation to one where the nucleon-nucleon cross section depends exclusively on the energy of the collision, following Ref. [23, 24]. The values of the cross section corresponding to the center-of-mass energies comprising this study are presented in Table I. This modification was implemented so that the AMPT and hydrodynamic calculations would start with identical initial geometries. We ran ap-

TABLE I. Nucleon-nucleon cross section as a function of collision energy in the Monte Carlo Glauber model.

$\sqrt{s_{NN}}$ [GeV]	σ_{NN} [mb]
7.7	31.2
20.0	32.5
39.0	34.3
62.4	36.0
200.0	42.3
5020.0	60.3

proximately 4 million central d +Au AMPT events at the highest energy and 8 million at the lowest energy, with impact parameter $b < 2$ fm. We have used the same geometry selection for all model calculations, so they are directly comparable, even though later comparison with experimental d +Au energy scan data may require further matching to experiment-specific centrality selections. In the case of AMPT, the matching is straightforward in that one can select on multiplicity or energy in the same pseudorapidity as the experiments and determine comparable centrality quantiles—as done for example in Ref. [25].

It has been shown that a partonic cross section of $\sigma_{part} = 1.5$ mb can reasonably reproduce the measured v_2 up to $p_T \approx 1$ GeV/c in d +Au and ^3He +Au at RHIC energies [17]. Hence, in keeping with these studies, we use the identical partonic cross section for all collision energies. It is important to note that our assumption of a constant cross section, independent of the collision energy, has been warranted by studies demonstrating how the same value of $\sigma_{part} = 1.5$ mb can reproduce flow observables in p + p and p +Pb at LHC energies [15].

For every AMPT event, we access the initial coordinates (r_i, ϕ_i) of the participant nucleons and smear them by a Gaussian of $\sigma = 0.4$ fm. We then compute the second and third order participant plane as follows

$$\Psi_n = \frac{\arctan[\langle r^2 \sin(n\phi) \rangle / \langle r^2 \cos(n\phi) \rangle]}{n} + \frac{\pi}{n}. \quad (2)$$

We calculate v_2 and v_3 for unidentified charged hadrons at midrapidity $|\eta| < 2$ according to Eq. (1). Calculating anisotropy moments in this manner has the advantage of excluding non-flow effects including resonance decays and jet fragmentation.

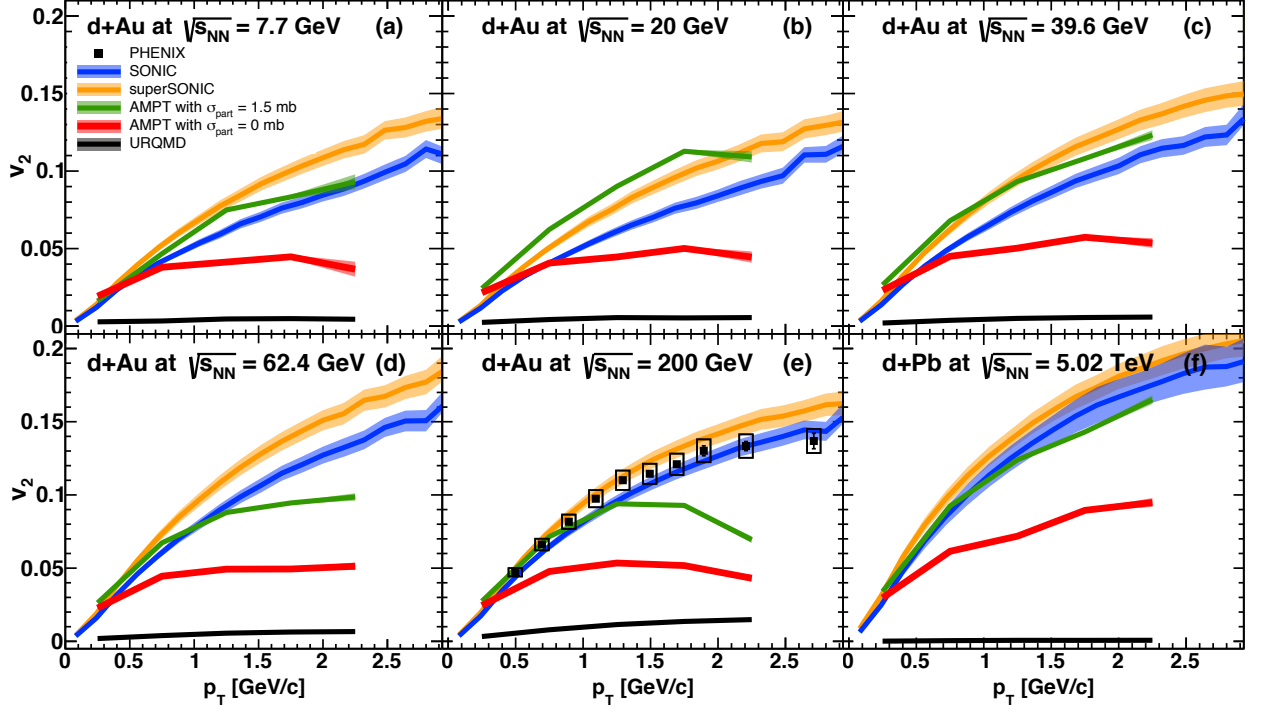


FIG. 1. Transverse momentum dependence of v_2 in $d+Au$ collisions at $\sqrt{s_{NN}} = 7.7, 20.0, 39.6, 62.4, 200.0$ GeV and in $d+Pb$ collisions at $\sqrt{s_{NN}} = 5.02$ TeV. Results are shown from viscous hydrodynamic calculations (SONIC and with pre-equilibrium dynamics SUPERSONIC) as well as the parton cascade model AMPT (with and without a partonic scattering stage), and the purely hadronic cascade model (URQMD). Published experimental data for v_2 in $d+Au$ at $\sqrt{s_{NN}} = 200$ GeV is also shown.

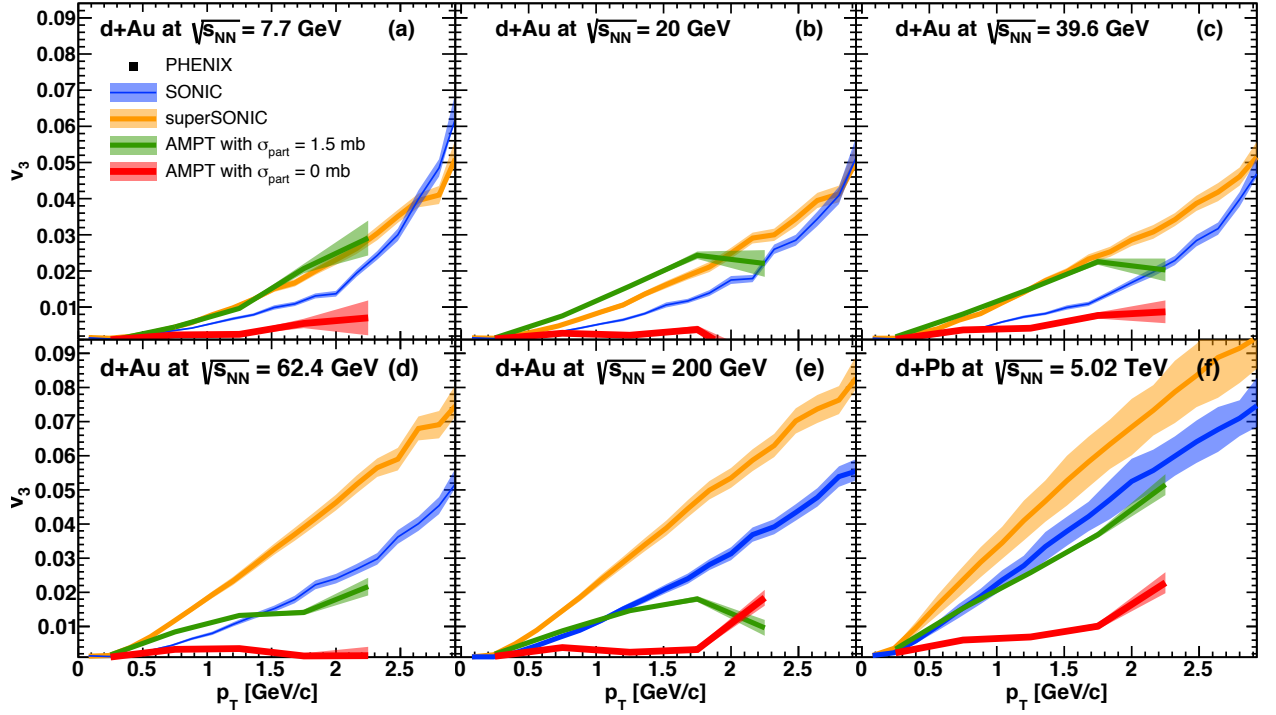


FIG. 2. Transverse momentum dependence of v_3 in $d+Au$ collisions at $\sqrt{s_{NN}} = 7.7, 20.0, 39.6, 62.4, 200.0$ GeV and in $d+Pb$ collisions at $\sqrt{s_{NN}} = 5.02$ TeV. Results are shown from viscous hydrodynamic calculations (SONIC and with pre-equilibrium dynamics SUPERSONIC) as well as the parton cascade model AMPT (with and without a partonic scattering stage).

We have also run AMPT with the partonic cross section set to zero ($\sigma_{part} = 0.0$ mb). In this case, one can isolate the effects of hadronization and the subsequent hadron cascade on the development of v_n . One can hypothesize that at some lower collision energy for small systems there is no partonic stage. In that case, experimental results might move from agreement with AMPT with $\sigma_{part} = 1.5$ mb at higher energy, towards the AMPT with $\sigma_{part} = 0.0$ mb (i.e. with no partonic stage) at lower energy.

B. URQMD

In order to further check expectations that for small systems at lower energies the medium is purely hadronic, we have also employed the URQMD model. The URQMD model Version 3.4 [26] is a hadronic transport model where initial nucleon positions are determined from a Woods-Saxon distribution. Hadrons, predominantly arising from strings are propagated via relativistic Boltzmann transport. As with AMPT, we modified the URQMD code to sample deuteron nucleon coordinates from the appropriate Hulthén wave function of the nucleus. The URQMD cutoff time for interactions was set to $t_{cutoff} = 20$ fm/c. Since the URQMD model was originally designed for the study of heavy ion collisions at energies between those of SIS and RHIC, the default model does not apply to LHC energies. In that case, care must be taken to compile the source code in LHC mode prior to running any calculation.

It is interesting to compare the results from AMPT with no partonic scattering to those from URQMD. In AMPT, as detailed above, the use of a standard Monte Carlo Glauber allows for a straightforward determination of the participant nucleons and the subsequent calculation of v_n relative to their symmetry plane, thus excluding any possible non-flow effects from the measured signal. On the other hand in URQMD, although initial nucleon coordinates are sampled from an appropriate description of the colliding nuclei, participants are not determined from the initial impact, but rather from the evolution of the system, as nucleons are struck over time by other nucleons or—more commonly—by the products of previous inelastic collisions. This results in an ambiguity in the definition of the URQMD participant plane. Through careful study, we find that a reliable participant plane Ψ_n can be extracted by including only nucleons struck by other nucleons or by restricting the interactions to occur at early times.

The URQMD calculations in Ref. [19] use the two-particle cumulant method [27] with an imposed pseudorapidity gap of $|\Delta\eta| > 0.2$ and > 0.8 . In order to cross check their results, we have implemented the two-particle cumulant method with varying pseudorapidity gaps. In addition, in order to extract v_n from URQMD minimizing non-flow contributions, we implemented four-particle cumulants following Ref. [27]. It was found that

$c_2\{4\} > 0$, resulting in a complex normalization for v_2 . It has been reported that this is a limitation of the method when dealing with large fluctuations in low multiplicity events [20].

C. Hydrodynamics

In the viscous hydrodynamic SONIC model, initial conditions are generated for each event using the identical Monte Carlo Glauber procedure described above for AMPT. These conditions are then translated into fluid cells propagated with 2+1 dimensional conformal viscous hydrodynamics as described in Ref. [12]. Lastly, final-state interactions are modeled with the hadronic cascade code B3D [28].

The SONIC implementation of viscous hydrodynamics has been successfully applied to A+A collisions at RHIC. However, it incorporates no pre-equilibrium dynamics. These are implemented in an extension of the model, known as SUPERSONIC [14]. In the latter, the AdS/CFT correspondence is used to derive a relation between the gradient of the initial energy density distribution and the radial dependence of fluid cell velocities, which accounts for the presence of pre-equilibrium dynamics. The final $v_n(p_T)$ are obtained by summing over final state particles, using the formalism described in Ref. [14].

III. RESULTS AND DISCUSSION

Figure 1 presents a full suite of theoretical predictions for elliptic anisotropy coefficients v_2 as a function of p_T for d +Au collisions at $\sqrt{s_{NN}} = 7.7, 20.0, 39.0, 62.4, 200.0$ GeV and 5.02 TeV. Experimental data in d +Au at $\sqrt{s_{NN}} = 200$ GeV for v_2 measured by the PHENIX collaboration is shown in panel (e). Similar predictions for v_3 are shown in Figure 2. We now discuss each category of predictions and possible implications for future measurements.

A. Hydrodynamics

In the context of hydrodynamics, there is a well-understood physical picture of how initial inhomogeneities in the energy density deposition due to intrinsic geometry or fluctuations are translated into final-state momentum anisotropies. This model has been successfully applied to large collision systems. In such cases, the duration of the QGP phase is long enough to bring the v_n signal from the hydrodynamic phase to saturation and dominate over other sources of flow prior to thermalization or following hadronization. However, it is precisely the dominance of the hydrodynamic phase that needs to be revisited for small collision systems.

Results from hydrodynamics are shown as the blue (SONIC) and yellow (SUPERSONIC) curves. The system-

atic uncertainty bands are calculated from the sensitivity to the viscous second order corrections as detailed in Ref. [14]. Both calculation results for $d+Au$ at $\sqrt{s_{NN}} = 200$ GeV are in reasonable agreement with the experimental data. The additional effect on v_2 of pre-equilibrium flow in SUPERSONIC of +10% relative to SONIC cannot be discriminated with the current experimental and theoretical uncertainties.

At the LHC, there is experimental data in $p+Pb$ at $\sqrt{s_{NN}} = 5.02$ TeV [29] and a comparison with the SONIC calculation is shown in Figure 3. We observe a reasonable agreement between the hydrodynamic calculation and data, validating the model at LHC energies. Furthermore, we see that SONIC predicts a substantially larger v_2 in $d+Pb$ compared with $p+Pb$ collisions. A major ambiguity in the interpretation of LHC $p+p$ and $p+Pb$ results is the widely differing models of the initial geometry and their event-wise fluctuations. In contrast, in $d+Pb$ collisions the initial geometry is mostly determined by the positions of the two nucleons in the deuteron rather than in modeling the proton substructure and shape fluctuations. Specifically, the Monte Carlo Glauber calculated eccentricity and the IP-Glasma calculated eccentricity [30] differ by less than 10% in $d + A$ collisions and differ by more than 125% in $p + A$ collisions. Recently it has been suggested that the IP-Glasma calculation may be augmented by including shape fluctuations of the proton (not just size fluctuations) [31], adding another degree of freedom to the calculation. In contrast, with $d+Pb$ data one can pin down the medium properties since the initial conditions are much better constrained, and then use the fixed medium properties to better understand the initial conditions in $p+Pb$. Thus, despite technical obstacles, future $d+Pb$ running at the LHC should be seriously considered.

The calculation results for $d+Au$ collisions at lower energies 7.7 - 62.4 GeV show a similar rise in the v_2 with p_T , though with modestly reduced magnitude. Shown in Figure 4, panel (a) are the ratios of v_2 as a function of p_T for each energy to the value in $d+Au$ at $\sqrt{s_{NN}} = 200$ GeV. The v_2 magnitude decreases monotonically from the highest energy to the lowest $\sqrt{s_{NN}}$ with only modest p_T dependence. It is striking that in going from the LHC energy of 5.02 TeV to RHIC top energy of 200 GeV, there is an approximate 25-30% decrease in the v_2 and then between 200 GeV and the lowest energy of 7.7 GeV the decrease is only another 25-30%. Given that large decrease in the energy available to be deposited to create the hot fireball, why is there no strong collapse of the v_2 at the lower energies?

To shed further light on this question, we sum the space-time volume of all fluid elements hotter than the transition temperature for every time step in our hydrodynamic simulations. The result, plotted as a function of collision energy, is shown in Figure 5. We observe a five-fold increase in the summed volume between the lowest and highest energies. Even at $\sqrt{s_{NN}} = 7.7$ GeV there is a space-time volume of QGP of order $8 \text{ fm}^2 \Delta y \text{ fm/c}$. As a very rough picture, one can think of this as a $2 \text{ fm} \times$

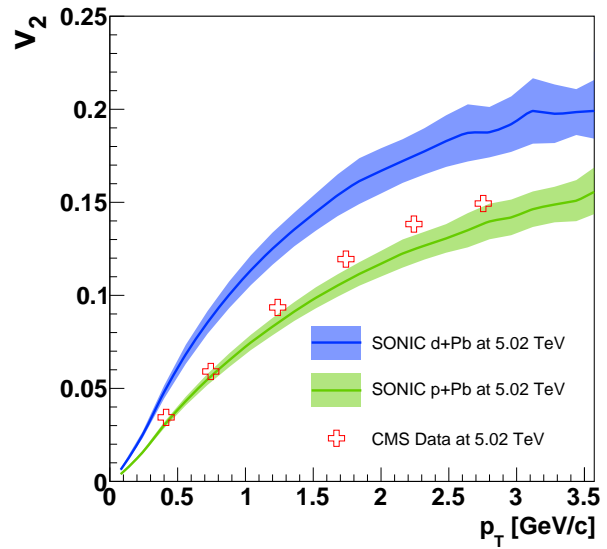


FIG. 3. Transverse momentum dependence of v_2 in $p+Pb$ and $d+Pb$ at $\sqrt{s_{NN}} = 5.02$ TeV from the SONIC hydrodynamic model. CMS measurements in central $p+Pb$ events are shown for comparison.

2 fm transverse area of QGP that lasts for a time 2 fm/c with rapidity interval Δy . Therefore, within the viscous hydrodynamics framework, the answer is that there is no minimum size to the QGP droplet. This makes sense since there is no expected first order phase transition with bubbles, but rather a continuous change where the space-time volume of the QGP simply decreases, playing a smaller and smaller role. Thus, even a rather small and short lived QGP phase is enough to quickly generate significant elliptic flow.

Figure 4, panel (b) shows the ratios of v_3 as a function of p_T for each energy to the value in $d+Au$ at $\sqrt{s_{NN}} = 200$ GeV. The v_3 calculation results show a much more dramatic drop with collision energy. The decrease in v_2 between 200 GeV and 7.7 GeV was 25-30%, but for v_3 the change is a reduction of roughly 300%. As noted in Ref. [10], the triangular flow simply takes a longer time to develop (i.e. to translate the spatial triangularity into momentum anisotropy) and thus it is natural that this signal is much more sensitive to the shorter and shorter QGP lifetime at the lower energies.

This effect is also quite striking when evaluating the influence of pre-equilibrium flow via the comparison of SONIC and SUPERSONIC. Shown in panel (a) of Figure 6 is the ratio of v_2 computed with SONIC to SUPERSONIC for all collision energies. For v_2 we see that the two calculations differ the most at the lowest energy, and are closest at the highest energy, with the ratio increasing monotonically with energy. This demonstrates that as the contribution of the hydrodynamic phase to total flow becomes weaker, pre-equilibrium dynamics play an increasingly significant role. The same ratio for v_3 is shown in panel

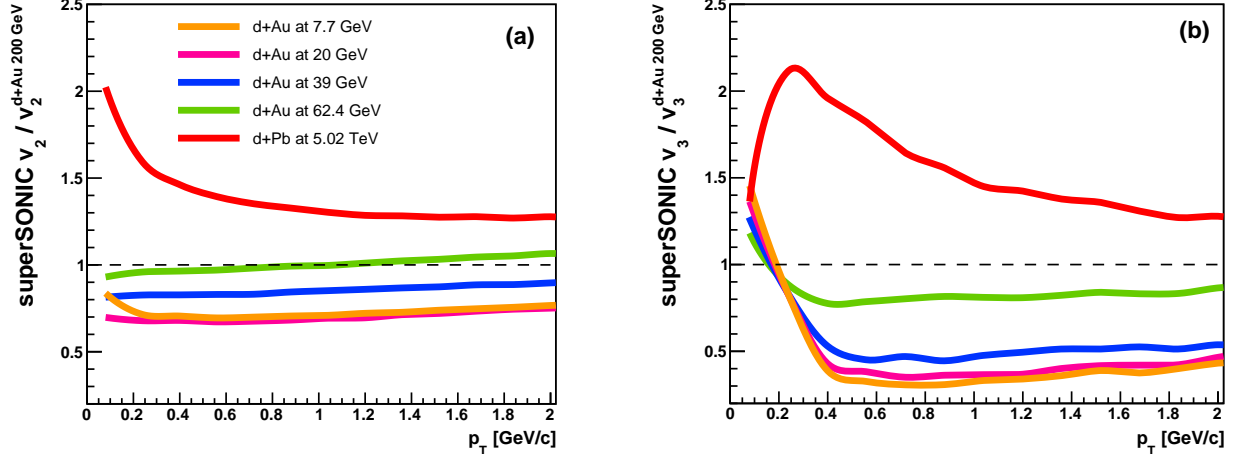


FIG. 4. Panels (a) and (b) show the ratio of v_2 (v_3) as a function of p_T at different energies to $d+\text{Au } v_2$ at $\sqrt{s_{NN}} = 200$ GeV from the SUPERSONIC hydrodynamic calculation.

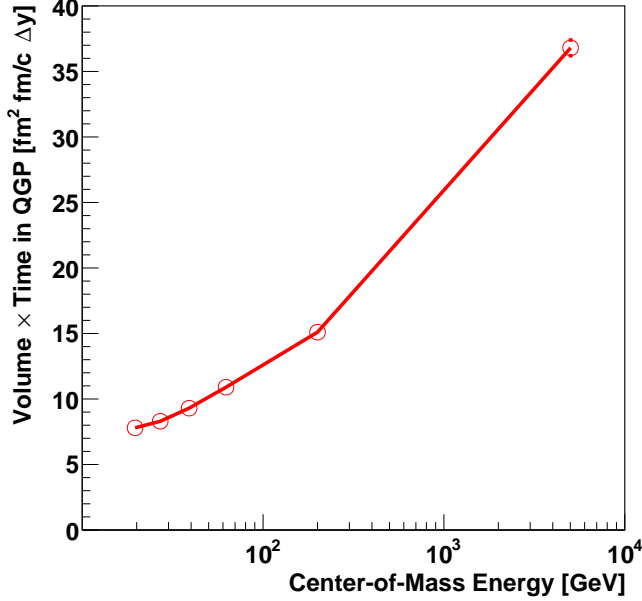


FIG. 5. Collision energy dependence of the summed space-time volume element in the QGP in viscous hydrodynamics.

(b). Pre-equilibrium also appears to play a stronger role in going from 5.02 TeV to 62.4 GeV. However, below that energy the v_3 values are quite small, less than 1% for $p_T < 1$ GeV/c, and the ratios no longer follow a monotonic trend. The best test of the influence of pre-equilibrium dynamics is with signals that take the longest time to develop, such as v_3 . It will also be very interesting to compare such experimental data in these small systems where the geometry is well quantified with recent results from the beam energy dependence of v_3 in

peripheral Au+Au collisions reported by the STAR collaboration [32].

B. Partonic versus Hadronic Scattering

We now discuss the results of AMPT with and without partonic scattering, and the purely hadronic model URQMD. AMPT results with $\sigma_{part} = 1.5$ mb are shown in green, and the results with no partonic scattering $\sigma_{part} = 0$ mb are shown in red for v_2 in Figure 1 and for v_3 in Figure 2. Across collision energies, calculations using AMPT with $\sigma_{part} = 1.5$ mb yield a sizable v_2 that grows as a function of p_T . The magnitude of v_2 decreases modestly with decreasing collision energy. The AMPT calculations with partonic scattering agree with the experimental data for $d+\text{Au}$ at 200 GeV up to $p_T \approx 1$ GeV/c and then decrease at higher p_T .

It is striking that AMPT can yield v_2 values comparable to hydrodynamics—see for example Ref. [33]. Previous studies have shown that, in small systems at $\sqrt{s_{NN}} = 200$ GeV, incoherent partonic scattering only accounts for approximately half of the total developed v_2 , with the remainder arising from coalescence and hadronic interactions [17]. As shown in Figure 7, the v_2 results decrease by approximately 25-30% from 5.02 TeV to 200 GeV, and then another 25-40% from 200 to 20 GeV - quite similar in magnitude to the effect in the hydrodynamic calculations. In order to study how partonic scattering in AMPT changes as a function of collision energy, Figure 8 shows the probability of a (anti)quark to undergo N scattering events prior to freeze out. It is noteworthy that over 50% of the quarks do not scatter at all, and the remainder scatter only a few times. It is seen that for $d+\text{Au}$, the probability of not scattering increases monotonically with collision energy. However, the dependence of this effect on $\sqrt{s_{NN}}$ is found to be small, of order 10%.

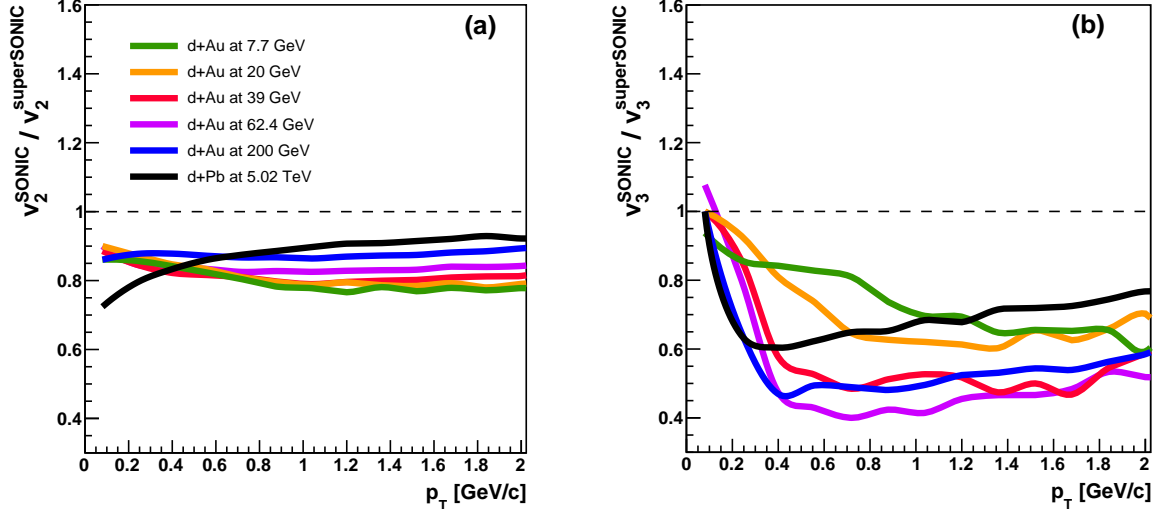


FIG. 6. Ratio of $v_2(p_T)$ in panel (a) and $v_3(p_T)$ in panel (b) from SONIC to SUPERSONIC for $d+Au$ at all collision energies.

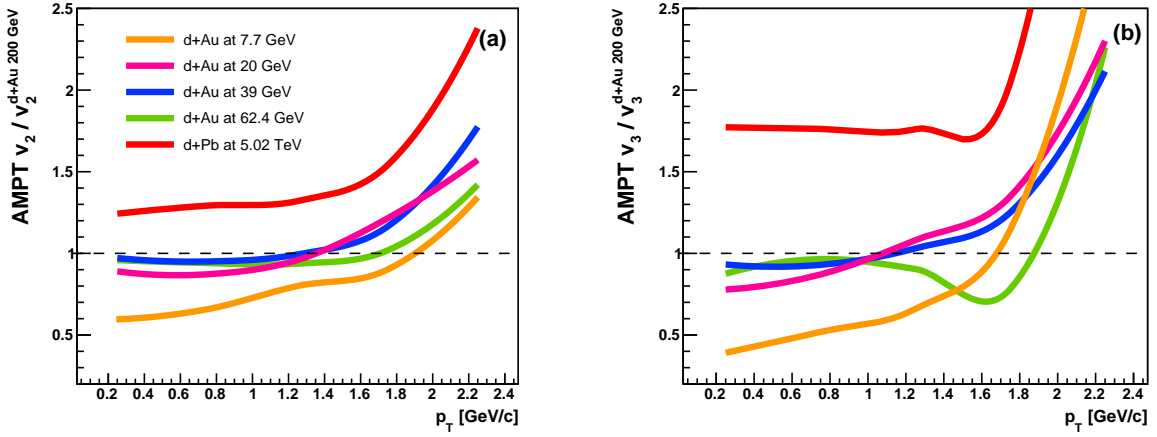


FIG. 7. Panels (a) and (b) show the ratio of v_2 and v_3 , respectively, as a function of p_T at different energies to $d+Au$ v_2 and v_3 at $\sqrt{s_{NN}} = 200$ GeV from AMPT.

In order to isolate the effects of hadronization and the subsequent hadron cascade on the development of v_n , AMPT was run with $\sigma_{part} = 0$ mb (i.e. with no partonic scattering). By setting the partonic cross section to $\sigma_{part} = 0$ mb, it is possible to turn off partonic scattering, such that azimuthal anisotropies develop from string melting, coalescence, and hadronic scattering. From Figure 1, we see that this hadronic phase accounts for approximately half of the v_2 signal above $p_T \approx 1$ GeV/c, regardless of collision energy. However, Figure 2 shows that the hadronic phase plays a more substantial role in the development of v_2 than it does v_3 . In all cases the reduction in flow coefficients is substantial, of order 50% for v_2 and even larger for v_3 where there is a complete collapse of triangular anisotropies without partonic scattering.

tering.

Additionally, the purely hadronic URQMD results for v_2 are shown in black in Figure 1. The URQMD results exhibit an extremely small v_2 that rises modestly with p_T . Both AMPT without partonic scattering and URQMD results fail to reproduce the experimental data in $d+Au$ collisions at 200 GeV. It is notable that these two calculations with hadronic rescattering only give quite different v_2 values. This means that the details of initial hadronic production play a large role in addition to the hadronic rescattering itself.

One hypothesis is that below some size and initial energy deposition, the system can be described as purely hadronic. If that regime is reached in lower collision energy $d+Au$ reactions, one might expect a significant decrease in the v_2 and a collapse of the v_3 in future lower

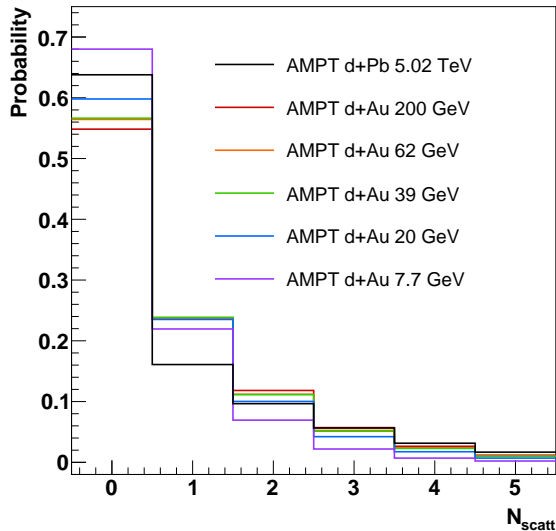


FIG. 8. Probability for a parton in AMPT to undergo N scattering events prior to hadronization, for d +Au and d +Pb collisions at a variety of collision energies.

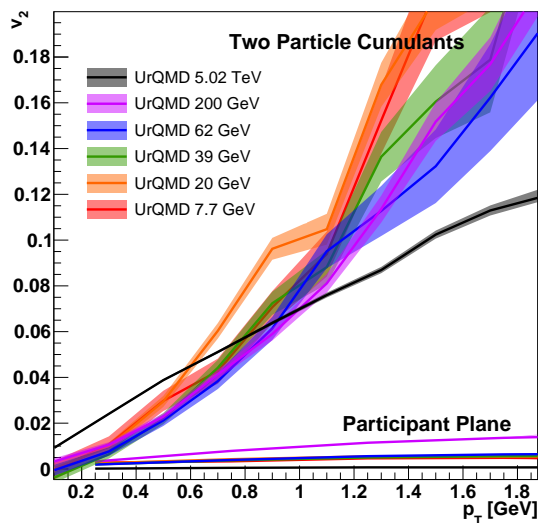


FIG. 9. Transverse momentum dependence of v_2 from the UrQMD model at variety of collision energies, computed with two-particle cumulants and with respect to the participant plane.

energy d +Au experimental results. This will be an important test of where partonic effects are no longer important.

Lastly, it is striking that the UrQMD v_2 results relative to the initial event plane are so small. In Ref. [19],

they use two-particle cumulants and find a substantial “flow” signal, though they attribute some of the effect to non-flow effects in comparing pseudorapidity gaps of $|\Delta\eta| > 0.2$ and $|\Delta\eta| > 0.8$. Shown in Figure 9 are our calculation results for the UrQMD participant event plane results and the two-particle cumulant results (in our case with $|\Delta\eta| > 1.6$) in d +Au collisions at various energies. The two-particle cumulant results are dramatically larger, have a very steep rise with p_T , and are actually largest for the lowest d +Au collision energy. All of these observations indicate a complete dominance of non-flow contributions, and thus warrant future caution in the use of two-particle cumulants alone.

IV. SUMMARY

Recent analyses of RHIC and LHC data have opened the door to the possibility of QGP formation in small systems, a regime where it had been previously given limited consideration. Although the role of initial geometry has been established, a beam energy scan would provide insight into the role of pre-equilibrium dynamics, partonic interactions, and hadronic interactions in the development of flow in these systems.

We find that both hydrodynamics (SONIC and SUPERSONIC) and AMPT predict a substantial v_2 and v_3 at all collision energies under consideration. Within hydrodynamics there is still a significant summed space-time volume of QGP even at the lowest energies, indicating the absence of a sharp turn off in the translation of initial state anisotropies to the final state in small systems. In AMPT, varying $\sqrt{s_{NN}}$ has only a modest impact on the dynamics of partonic scattering. Results from AMPT without partonic scattering and the purely hadronic UrQMD indicate that if at lower energies the system is purely hadronic, one would expect a significant drop in v_2 observed via a small system beam energy scan. New experimental data from the small system beam energy scan at RHIC can shed new light on the required dynamics in these collisions with shorter and shorter lifetimes.

ACKNOWLEDGMENTS

We gratefully acknowledge Paul Romatschke for providing us with the SONIC and SUPERSONIC curves. We also acknowledge useful discussions on UrQMD with Steffen Bass, Hannah Petersen, Huichao Song, and You Zhou; and on AMPT with Zi-Wei Lin. We acknowledge funding from the Division of Nuclear Physics of the U.S. Department of Energy under Grant No. DE-FG02-00ER41152.

-
- [1] R. Snellings, *New J. Phys.* **13**, 055008 (2011).
 - [2] M. Luzum and P. Romatschke, *Phys. Rev.* **C78**, 034915 (2008), [Erratum: *Phys. Rev.* **C79**, 039903(2009)].
 - [3] A. Adare *et al.* (PHENIX), *Phys. Rev. Lett.* **114**, 192301 (2015).
 - [4] B. Abelev *et al.* (ALICE Collaboration), *Physics Letters B* **719**, 29 (2013).
 - [5] G. Aad *et al.* (ATLAS Collaboration), *Phys. Rev. Lett.* **110**, 182302 (2013).
 - [6] S. Chatrchyan *et al.* (CMS Collaboration), *Physics Letters B* **718**, 795 (2013).
 - [7] L. Adamczyk *et al.* (STAR), *Phys. Lett.* **B743**, 333 (2015).
 - [8] G. Aad *et al.* (ATLAS), (2015), arXiv:1509.04776 [hep-ex].
 - [9] V. Khachatryan *et al.* (CMS), (2015), arXiv:1510.03068 [nucl-ex].
 - [10] J. L. Nagle, A. Adare, S. Beckman, T. Koblesky, J. O. Koop, D. McGlinchey, P. Romatschke, J. Carlson, J. E. Lynn, and M. McCumber, *Phys. Rev. Lett.* **113**, 112301 (2014).
 - [11] A. Adare *et al.* (PHENIX), *Phys. Rev. Lett.* **115**, 142301 (2015).
 - [12] M. Habich, J. L. Nagle, and P. Romatschke, *Eur. Phys. J.* **C75**, 15 (2015).
 - [13] Itaru Nakagawa for the PHENIX Collaboration, ““PHENIX results on collectivity tests in high-multiplicity p+p and p+Au collisions”,” https://indico.cern.ch/event/355454/session/31/contribution/378/attachments/1161579/1672731/QM2015_itaru_150929_v1.1.pdf, the XXV International Conference on Ultrarelativistic Nucleus-Nucleus Collisions. September 27 - October 3. Kobe, Japan (Unpublished).
 - [14] P. Romatschke, *Eur. Phys. J.* **C75**, 305 (2015).
 - [15] G.-L. Ma and A. Bzdak, *Physics Letters B* **739**, 209 (2014).
 - [16] A. Bzdak and G.-L. Ma, *Phys. Rev. Lett.* **113**, 252301 (2014).
 - [17] J. D. Orjuela Koop, A. Adare, D. McGlinchey, and J. L. Nagle, *Phys. Rev.* **C92**, 054903 (2015).
 - [18] L. He, T. Edmonds, Z.-W. Lin, F. Liu, D. Molnar, and F. Wang, “Anisotropic parton escape is the dominant source of azimuthal anisotropy in transport models,” (2015), arXiv:1502.05572 [nucl-th].
 - [19] Y. Zhou, X. Zhu, P. Li, and H. Song, *Phys. Rev.* **C91**, 064908 (2015).
 - [20] X. Zhu, M. Bleicher, and H. Stöcker, *Phys. Rev. C* **72**, 064911 (2005).
 - [21] Z.-W. Lin, C. M. Ko, B.-A. Li, B. Zhang, and S. Pal, *Phys. Rev. C* **72**, 064901 (2005).
 - [22] X.-N. Wang and M. Gyulassy, *Computer Physics Communications* **83**, 307 (1994).
 - [23] M. L. Miller, K. Reygers, S. J. Sanders, and P. Steinberg, *Ann. Rev. Nucl. Part. Sci.* **57**, 205 (2007).
 - [24] C. Loizides, J. Nagle, and P. Steinberg, (2014), arXiv:1408.2549 [nucl-ex].
 - [25] A. Adare *et al.* (PHENIX), (2015), arXiv:1509.07758 [nucl-ex].
 - [26] S. A. Bass *et al.*, *Prog. Part. Nucl. Phys.* **41**, 255 (1998), [*Prog. Part. Nucl. Phys.* **41**, 225(1998)].
 - [27] A. Bilandzic, R. Snellings, and S. Voloshin, *Phys. Rev.* **C83**, 044913 (2011).
 - [28] J. Novak, K. Novak, S. Pratt, J. Vredevoogd, C. Coleman-Smith, and R. Wolpert, *Phys. Rev.* **C89**, 034917 (2014).
 - [29] S. Chatrchyan *et al.* (CMS), *Phys. Lett.* **B724**, 213 (2013).
 - [30] B. Schenke and R. Venugopalan, *Proceedings, 24th International Conference on Ultra-Relativistic Nucleus-Nucleus Collisions (Quark Matter 2014)*, *Nucl. Phys.* **A931**, 1039 (2014).
 - [31] S. Schlichting and B. Schenke, *Phys. Lett.* **B739**, 313 (2014).
 - [32] L. Adamczyk *et al.* (STAR), (2016), arXiv:1601.01999 [nucl-ex].
 - [33] A. Adare *et al.* (PHENIX), (2015), arXiv:1509.06337 [nucl-ex].